15th Seminar "New Trends in Research of Energetic Materials", Part II, pp. 475-484, ISBN 978-80-7395-480-2, University of Pardubice, Pardubice, Czech Republic, April 18–20, 2012.

Numerical simulations for prediction of aerodynamic drag on high velocity fragments from naturally fragmenting high explosive warheads

Alan Catovic*, Berko Zecevic*, Sabina Serdarevic Kadic*, Jasmin Terzic*

* University of Sarajevo, Mechanical Engineering faculty, Bosnia and Herzegovina
e-mail: catovic@mef.unsa.ba

Abstract:

Numerical simulation of airflow around several representative high velocity fragments, originating from naturally fragmenting HE warhead 130mm M79, was performed using FLUENT® finite element method package.

FLUENT® software contains the broad physical modeling capabilities needed to model flow, turbulence, heat transfer for different applications, ranging from air flow over an aerodynamic surface to real combustion processes.

Aerodynamic drag coefficients of fragments were predicted for a wide range of Mach numbers (0.2, 0.4, 0.6, 0.8, 1, 1.1, 1.2, 1.3, 1.5, 2, 3, 4 and 5 Ma) and for eight different positions of fragments (0°, 45°, 90°, 135°, 180°, 225°, 270°, i 315°).

Different positions simulate dynamic instability of fragments during their flight through the atmosphere and account for stochastic behavior of fragments, which directly influences aerodynamic drag coefficients, fragments range and warhead lethal zones.

Obtained results of aerodynamic drag coefficients were compared with available experimental data.

Keywords: numerical simulation, fragment, FLUENT ®, drag coefficient;

1 Numerical simulation

Over 500 numerical simulations of high speed external aerodynamic flow over projectile fragments were performed in Fluent®. Simulations were performed on 4-processor computer.

Aim of the research was to predict range and variations of aerodynamic drag coefficient C_d for real rotating fragments with different mass and velocities.

Fragments used represent real fragments (fig. 1) from detonating HE projectile 130mm M79. Using Pit tests it was determined that during natural fragmentation of projectile 130mm M79 around 4000 do 6800 fragments were formed. [2]

Gurney method for different sections of projectile 130mm M79 was used to determine initial velocity of fragments variations from 1,2 Ma to 3 Ma [6], where Mach number (Ma) is dimensionless number representing the ratio of speed of an object moving through air to the local speed of sound.

Simulations were carried out for different fragment masses, different Ma numbers (0.2, 0.4, 0.6, 0.8, 1, 1.1, 1.2, 1.3, 1.5, 2, 3, 4 and 5 Ma) and different angles of atack (0°, 45°, 90°, 135°, 180°, 225°, 270°, 315°) that simulated rotation of fragment and its dynamic instability during the flight (fig. 2).

Verification of numerical model used was performed on a sphere and obtained results were compared to experimental data [20]. Values of drag coefficient for sphere obtained from simulation differed 2,6% compared to experimental data for sphere velocity of 1,2 Ma, 1,6% for 1,5 Ma, 9,3% for 2 Ma and 1,4% compared to experimental data for sphere velocity of 3 Ma.

Fragments were scanned and digitized in Autodesk AutoCAD®, based on their real geometry (fig. 3). Fragments were defined as two-dimensional bodies with constant depth, determined from fragments real mass and surface area in flow plane (plane XY in fig. 3)

This approach is somewhat similar to McCleskey model [10] where average fragment depth was determined using fragment mass and its equivalent surface area - approximated with square. Our model, however, uses advantages of CAD systems in defining real area of irregular surfaces, since approximation of fragment shape with known geometric objects (cube, sphere, cyllinder, parallelepiped) can lead to larger errors in prediction of aerodynamic drag.

Figure 1: Real fragments photographs
(from above: m < 1g, 1 - 2g, 2 - 3g, 30 - 50g, 50 - 100g)

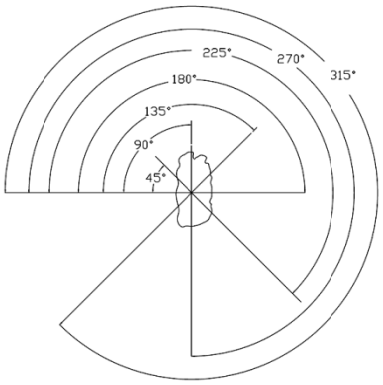

Figure 2: Scheme of airflow model

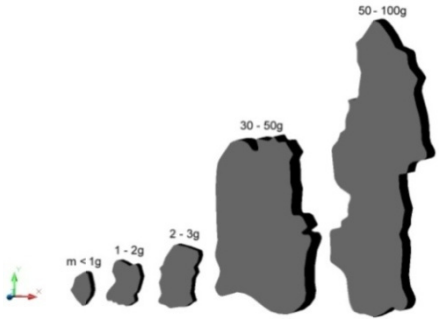

Figure 3: Digitized fragments

In table 1 mass and geometric parameters of fragments were presented.

Table 1: Mass and geometric parameters of fragments

mass group of fragments	fragment mass (g)	fragment surface area in flow plane (mm^2)	fragment depth (mm)	principal moments of inertia ($kgmm^2$)		
				Ix	Iy	Iz
<1g	0,7	28,8611	3,089	0,003066	0,001621	0,003574
1-2g	1,4	61,7891	2,886	0,012157	0,005891	0,016109
2-3g	2,7	109,113	3,152	0,046990	0,015310	0,057824
30-50g	46,9	763,091	7,829	5,758494	1,833481	7,114241
50-100g	51,6	1046,11	6,283	16,95349	1,429911	18,04484

Dimensions of numerical mesh are specified according to criteria [1,3] that spatial domain around simulating body should be at least 10-20 maximal dimensions of the body model (fragment).

Numerical meshes were unstructured due to higly irregular fragment shape and refined around fragments (fig. 4).

In table 2 summary of model, solver, material, rezidual tolerance and solution control are given.

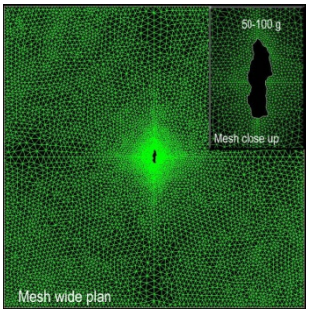

Figure 4: Unstructured mesh

Table 2: Summary of numerical simulation setup

Parameters	**Setup**
Flow:	Compressible (for Ma > 0,3) Turbulent (high Re numbers)
Solver:	Density based solver Steady, 2D, plannar
Turbulence model:	Spalart-Allmaras model [1], with constants: C_{b1} = 0,1355 C_{b2} = 0,622 C_v = 7,1 C_w =0,3
Material:	Air - Ideal gas: Specific heat C_p = 1006,43 J/kgK thermal conductivity k = 0,0242 W/mK Sutherland model for viscosity with three coefficients: $\mu_0 = 1{,}76 \cdot 10^{-5}$ kg/ms T_0 = 273,11 K S = 110,56 K
Boundary conditions:	Pressure and temperature defined at boundary limits Fragment - wall
Reference values:	Referent fragment area Pressure farfield
Method:	Implicit method: Spatial discretization: Gradient: Green-Gaus cell/node based Flow: Upwind second/first order Number of iteration: < 5000 (all solutions converged)
Solution controls:	Residual tolerance: 10^{-5} Courant number: variable, depending on convergence Under relaxation factors: Modified turbulent viscosity - 0,8 Turbulent viscosity - 1

2 Analysis and interpretation of results

Diagrams of characteristic curves C_d vs Ma for fragment with different mass are presented in figures 5-9.

Closer look at the curves reveal peak values of C_d for all fragments around 1 Ma. Largest changes of C_d values occur in transonic zone, as was expected [26,28]. For supersonic flow regimes (1,5 - 5 Ma), changes of C_d for different Ma numbers are smaller.

Drag coefficient C_d was determined using following equation from aerodynamics:

$$C_d = \frac{D}{q_\infty A}. \tag{1}$$

In (1) D is drag force, A is reference area and q_∞ dynamic pressure ($q_\infty = 0{,}5\rho_\infty v_\infty^2$) where variables ρ_∞ and v_∞ represent free stream density and velocity, respectively. [19]

In equation (1) reference area A is chosen to pertain to the given geometric body shape. For different shapes A may be different things. For an airplane wing, A is the planform area, and for sphere A is the cross-sectional area. Whenever using force coefficient data one must always know what reference quantities the particular data are based upon. [19]

In our work reference area A represents maximal exposed area of fragment normal to fragment velocity vector. It is the product of fragment depth and maximal dimension perpendicular to velocity vector (fig. 10).

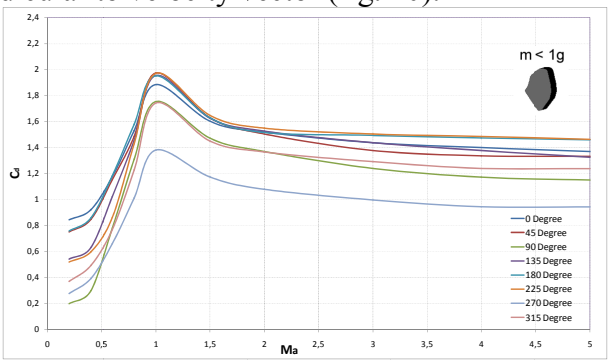

Figure 5: C_d vs Ma for mass group m< 1g

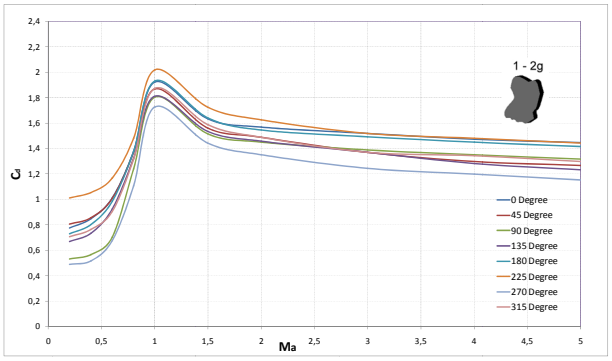

Figure 6: C_d vs Ma for mass group m=1-2g

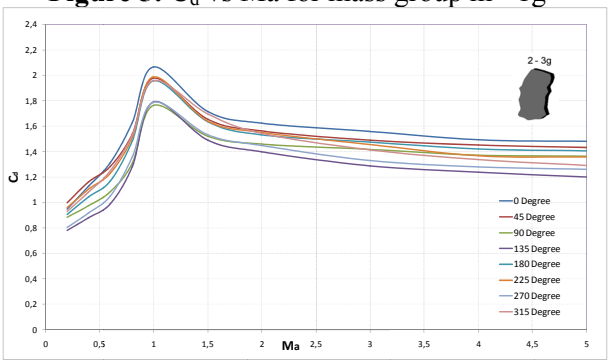

Figure 7: C_d vs Ma for mass group m=2-3g

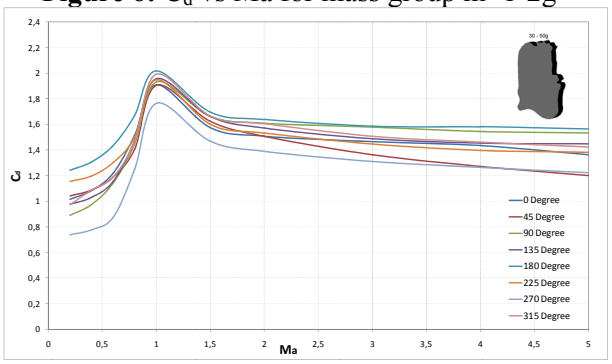

Figure 8: C_d vs Ma for mass group m=30-50g

In order to characterize the difference bebetween C_d values for fragments with different mass and velocities, a new parameter is introduced. We named it fragment slenderness and designated as λ.

Fragment slenderness λ was defined as ratio of fragment dimension parallel to velocity vector (b) and fragment dimension perpendicular to velocity vector (a), as in fig.10.

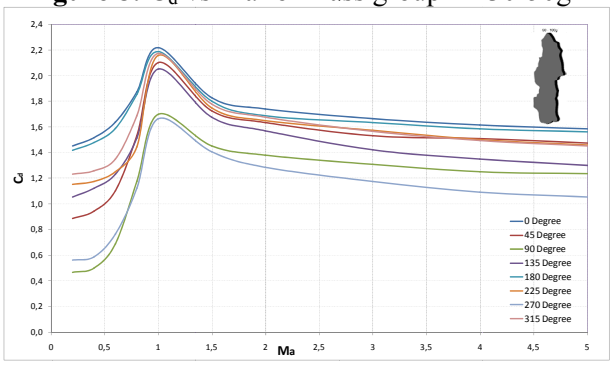

Figure 9: C_d vs Ma for mass group m=50-100g

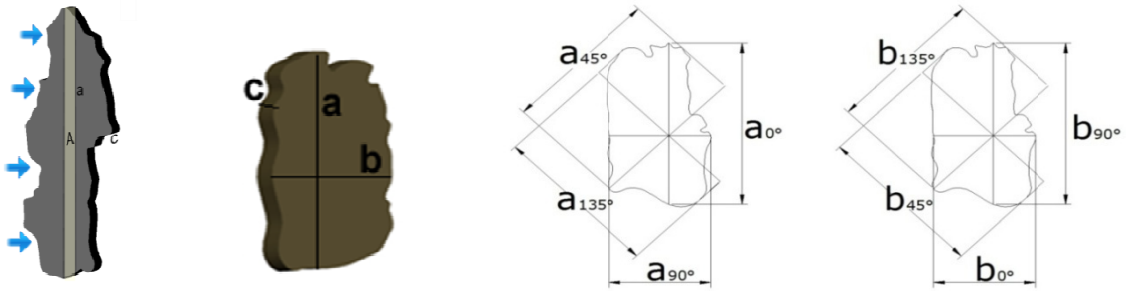

Figure 10: Reference area A and dimension of fragments for different angles of attack

In table 3 values of fragment slenderness λ are shown for different fragment mass and different angles of attack.

Table 3: Fragment slenderness λ

Angle of attack	m < 1g	m = 1-2g	m = 2-3g	m = 30-50g	m=50-100g (XY plane)	m = 50-100g (YZ plane)
	λ	λ	λ	λ	λ	λ
0°	0,658	0,783	0,662	0,548	0,343	0,171
45°	0,984	0,909	0,844	1,054	1,094	0,973
90°	1,518	1,276	1,510	1,826	2,924	4,375
135°	1,016	1,101	1,185	0,949	0,914	1,028

During the research numerical simulations of fragment (mass group 50-100g) rotated in vertical plane were performed (fig. 11). For the same fragment new slenderness is obtained (table 3), depending on the angle of attack.

Goal of this analysis was to investigate possible changes in C_d values for different flow planes of fragments.

After 3D rotation of fragments (now in YZ plane) reference area of fragment was increased, except for 90° angle of attack, where as expected lower values of C_d were obtained.

Results didn't show significant changes of C_d compared to flow over fragment in XY plane.

Largest differences occurred in subsonic zone, while for supersonic zone these difference decreased.

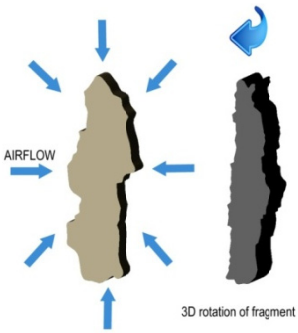

Figure 11: 3D rotation of fragment

Diagram in fig. 12 present curves C_d vs Ma for fragment with different slenderness λ.

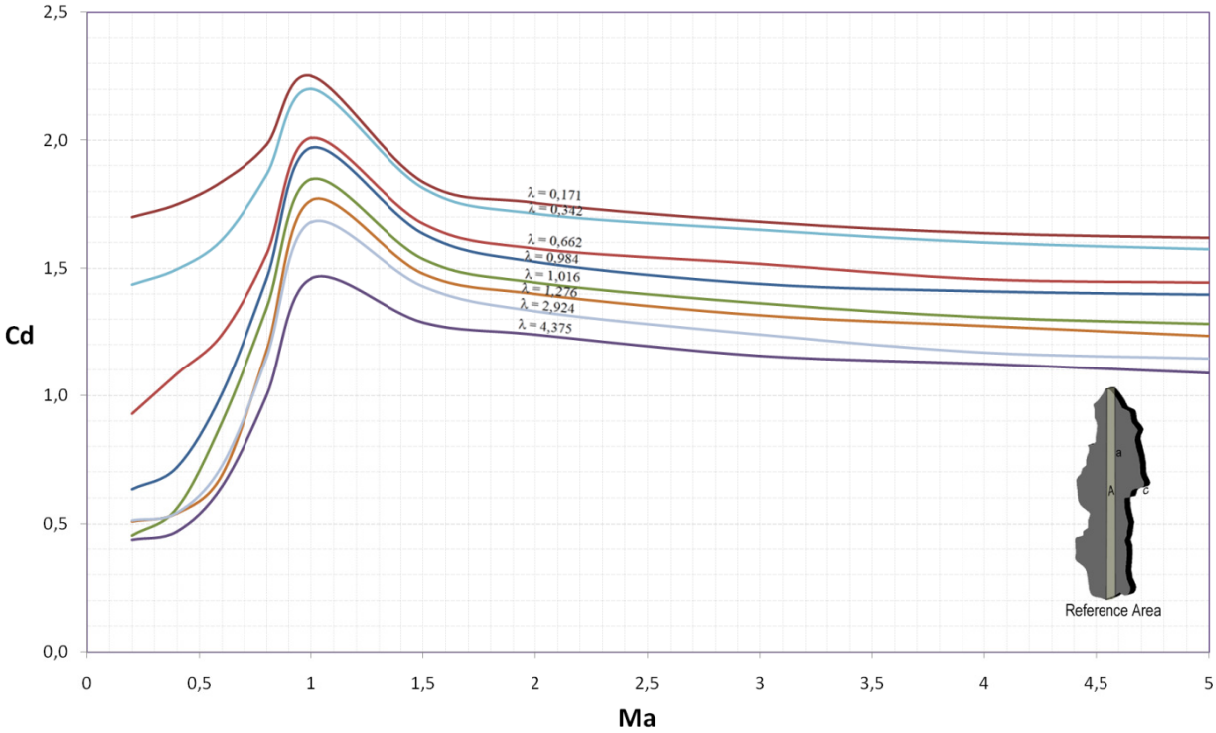

Figure 12: C_d vs Ma as a function of fragment slenderness λ

Using diagram in fig. 12 it is possible for known shape and velocity of fragment to predict its drag coefficient C_d. Fragments with highest slenderness have lowest drag coefficient C_d.

For fragments with slenderness λ = 4,375 and fragments with λ = 0,171, difference in C_d for velocity of 1 Ma is around 35% (fig. 12).

Fluent® was used to present pressure and Ma number fields around fragments (fig. 13, 14).

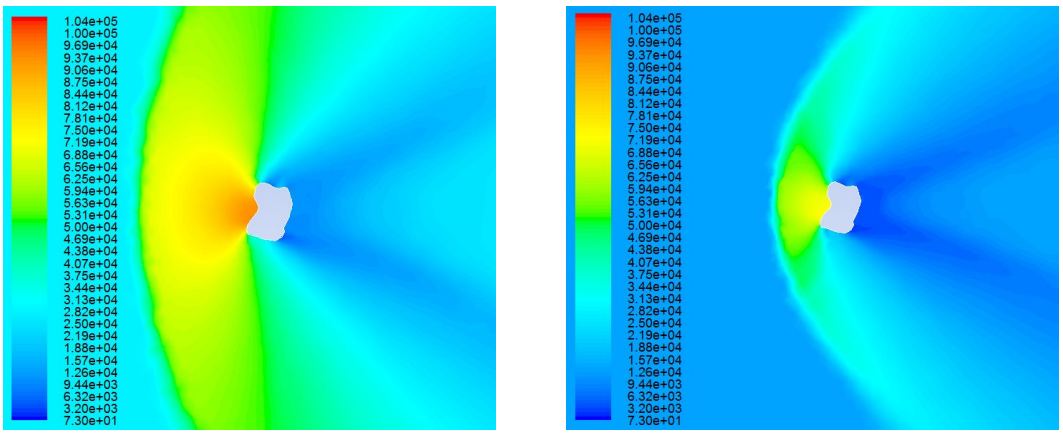

Angle of attack 0°, Ma = 1,5 *Angle of attack 0°, Ma = 2*

Angle of attack 0°, Ma = 3 *Angle of attack 0°, Ma = 4*

Figure 13: Pressure field for constant angle of atack and different fragment velocities

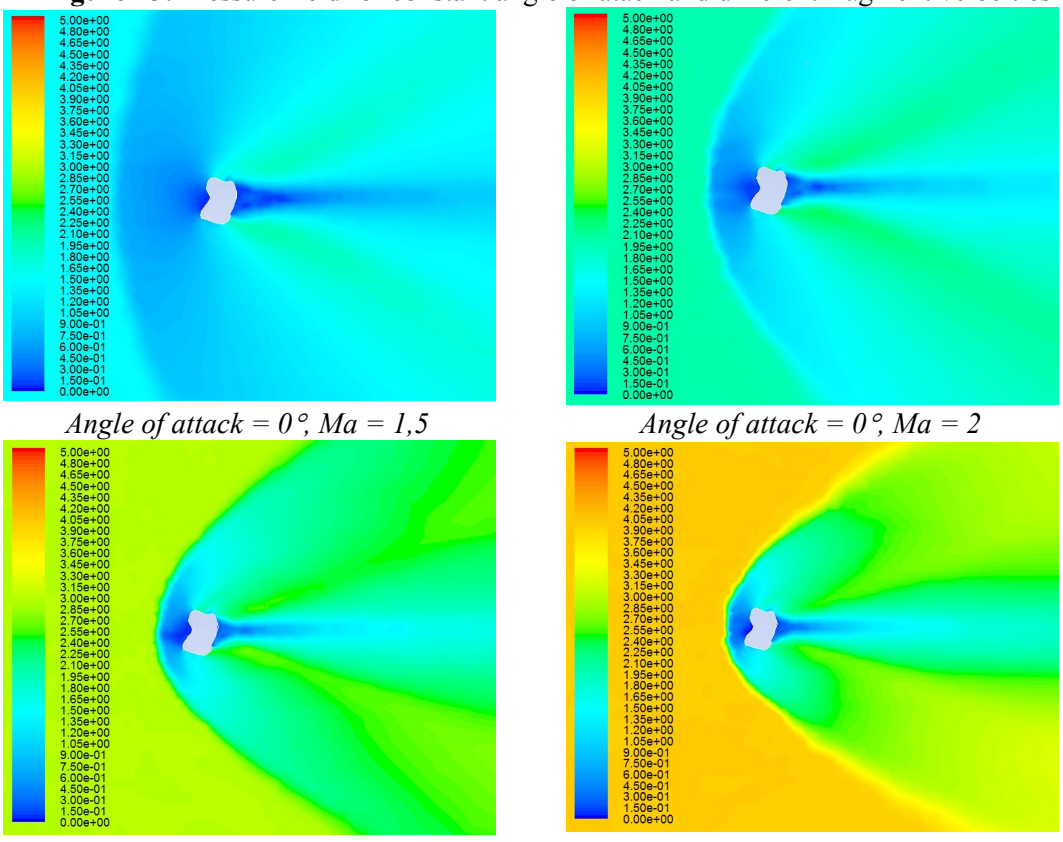

Angle of attack = 0°, Ma = 1,5 *Angle of attack = 0°, Ma = 2*

Angle of attack = 0°, Ma = 3 *Angle of attack = 0°, Ma = 3*

Figure 14: Ma number field for constant angle of attack and different fragment velocities

Pressure fields around fragment (m = 1-2 g) for constant angle of attack and different velocities (1,5 - 4 Ma) are presented in fig. 13. There is a zone of lower pressures behind the fragment and characteristic overpressure zone before the fragment. With increased velocity of fragments this zone is reduced (fig. 13).

Fig. 14 shows diagrams of Ma number fields around fragment for constant angle of attack and different velocities (1,5 - 4 Ma).

Supersonic flows are characterized by the presence of shock waves across which the flow properties and streamlines change discontinuously. Distinct expansion waves are common in supersonic flow.

For blunt bodies, such as fragment, the oblique shock wave will detach from the tip of the body, and will form strong curved bow shock ahead of a body with substantial region of subsonic flow behind the wave. [19] These effects are visible in fig. 14.

Diagrams in fig 15 show pressure field around fragment for constant Ma number and different attack angles for fragment m = 1-2 g. These diagram show variation of pressure around fragment for different angles of attack, simulating possible rotation of fragment during movement through the air.

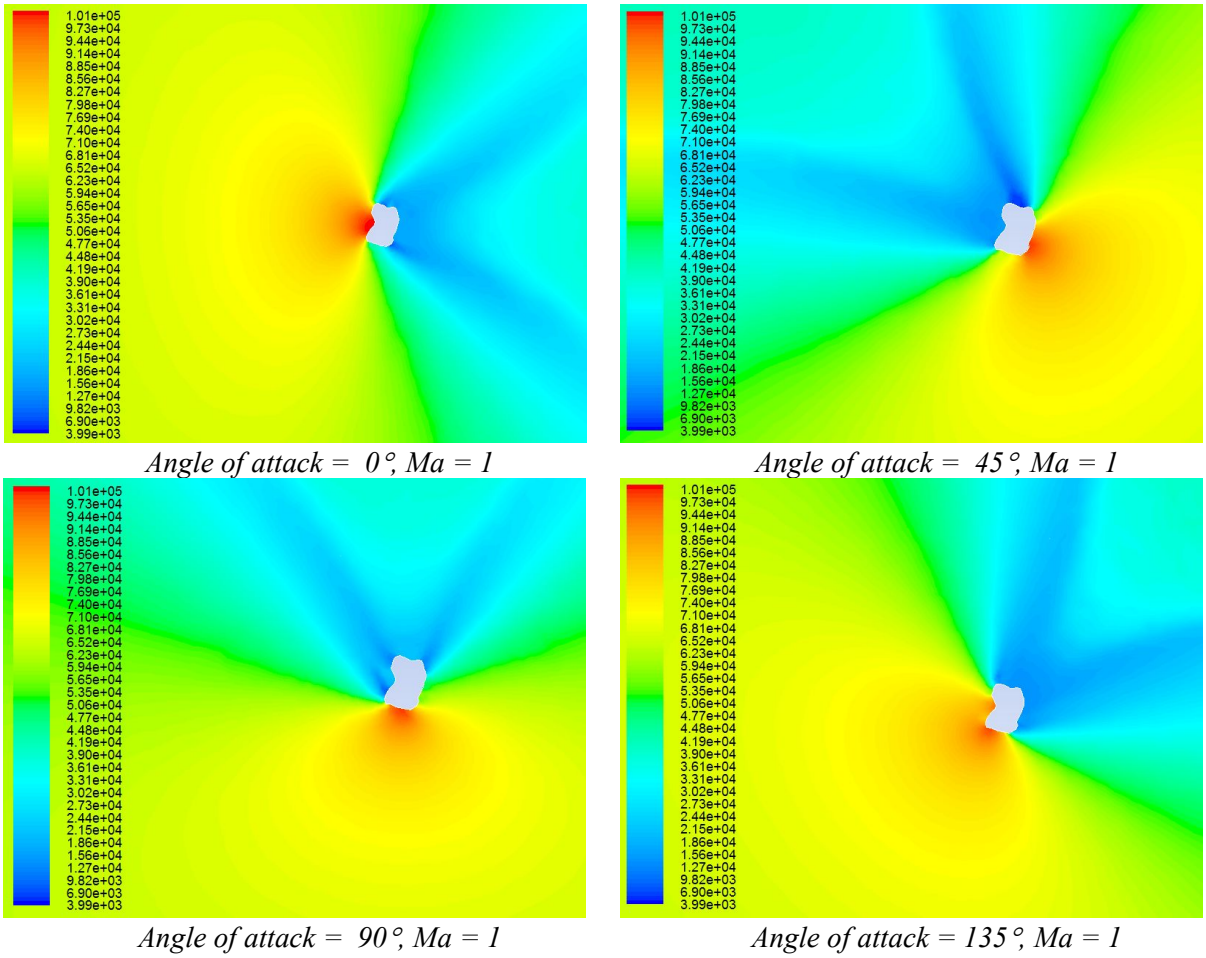

Angle of attack = 0°, Ma = 1 *Angle of attack = 45°, Ma = 1*

Angle of attack = 90°, Ma = 1 *Angle of attack = 135°, Ma = 1*

Figure 15: Pressure field around fragment for const Ma number and different attack angles (m=1-2g)

Diagrams in fig. 15 show that for fragments, with highly irregular surfaces, masses and shapes, every fragment will have unique pressure distribution for given velocity and attack angle.

Next step in analysis of pressure fields around moving fragments, for different angles of attack, will be defining the difference between center of pressure and center of mass in order to predict fragment overturning moment.

Comparation of numerical simulation results with available experimental data was conducted. There are very few publicly available data on aerodynamic parameters of fragments from HE projectiles. They are generally incomplete, with missing data about mass and dimension of fragments. Also many of available experimental research lack the test data on drag coefficient C_d for transonic and supersonic flow regimes.

Diagram in figure 16 presents comparation of numerical results data with available experimental data.

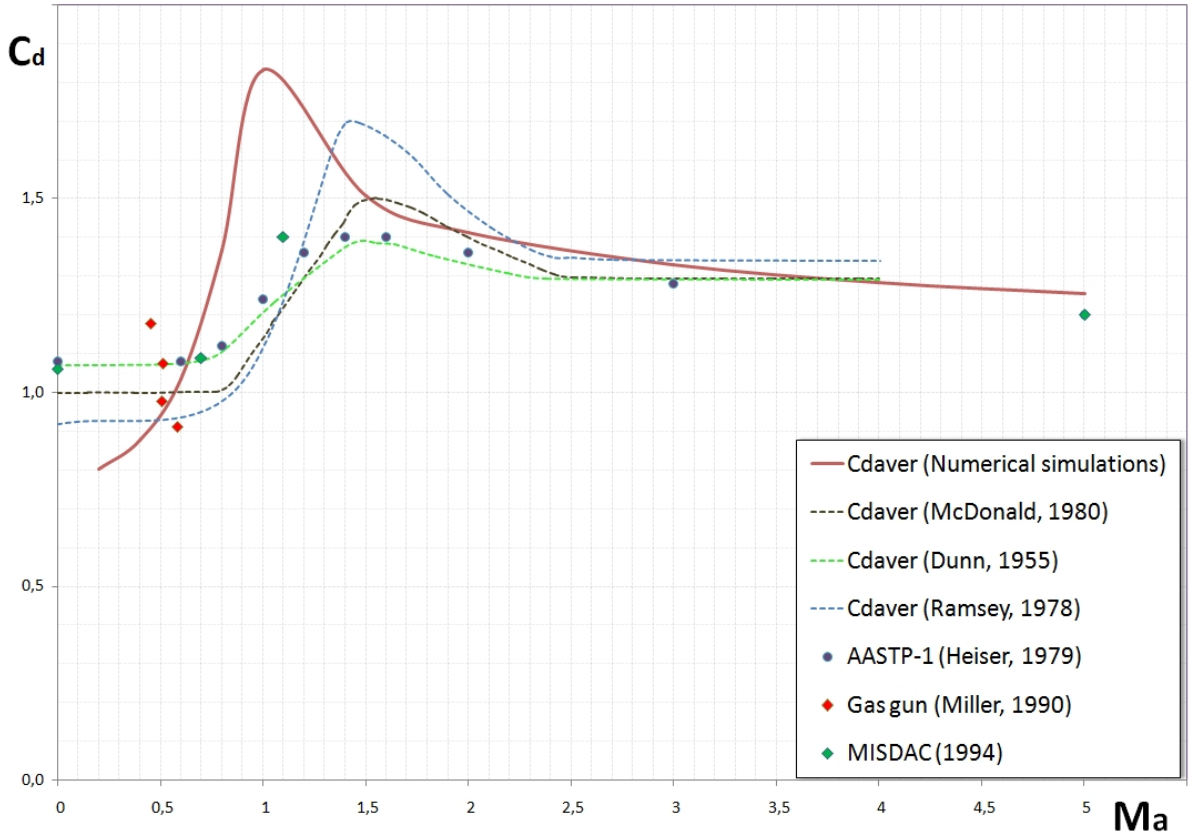

Figure 16: Comparation of numerical results with available experimental data [12,13,14,15,17,18]

Red curve C_d vs Ma presented in diagram (fig. 16) was obtained by averaging numerical simulation data for all fragments.

Best agreement between numerical and experimental data was obtained for supersonic flow regimes.

Significantly lower agreement was observed for transonic and subsonic data.

In our research curve C_d vs Ma, obtained from numerical simulation data, has its peak around 1 Ma, while for other available test data this peak was observed from 1,1 Ma [14] to 1,5 Ma [12, 13, 17,18]. This difference should be investigated in following research.

Table 4 shows difference between values of drag coefficient C_d from numerical simulation and experimental data, for supersonic flow regimes (1,5 – 5 Ma). Maximal relative difference between numerical simulation and experimental data was 12,8% at 1,5 Ma. For other Ma number these differences were significantly lower.

Presented numerical simulations were two-dimensional. In real case scenario fragment made by detonation of HE projectiles could position itself in any shape during its motion through the atmosphere since their total initial velocity generally depends on impact velocity of projectile, tangential velocity of projectile (for dynamically stabilized projectiles) and velocity component generated by high pressure detonating products.

Because of the complexity of mechanisms involved, further research is needed.

Table 4: Difference drag coefficient C_d from numerical simulation and experimental data

		Ma number				
		1,5	**2**	**3**	**4**	**5**
$\mathbf{C_{av\text{-}NS}}$ (Numerical simulations)		1,508	1,414	1,331	1,283	-
$\mathbf{C_{av\text{-}M}}$ (McDonald) [12]		1,497	1,383	1,294	1,293	-
$\mathbf{C_{av\text{-}D}}$ (Dunn, Porter) [17]		1,391	1,320	1,295	1,295	-
$\mathbf{C_{av\text{-}R}}$ (Ramsey, Smith, Powell) [18]		1,701	1,461	1,338	1,338	-
$\mathbf{C_{av\text{-}AASTP}}$ (AASTP-1) [13]		1,401	1,360	1,280	1,240	1,2
$\mathbf{C_{av\text{-}MISDAC}}$ (MISDAC) [14]		1,398	1,381	1,328	1,275	1,2
Relative difference (%)	$\mathbf{C_{av\text{-}NS}}$ / $\mathbf{C_{av\text{-}M}}$	0,746	2,183	2,711	0,819	-
	$\mathbf{C_{av\text{-}NS}}$ / $\mathbf{C_{av\text{-}D}}$	7,782	6,610	2,702	0,935	-
	$\mathbf{C_{av\text{-}NS}}$ / $\mathbf{C_{av\text{-}R}}$	12,80	3,286	0,560	4,320	-
	$\mathbf{C_{av\text{-}NS}}$ / $\mathbf{C_{av\text{-}AASTP}}$	7,160	3,788	3,798	3,320	4,292
	$\mathbf{C_{av\text{-}NS}}$ / $\mathbf{C_{av\text{-}MISDAC}}$	7,292	2,302	0,191	0,591	4,291

3 Conclusion

Large number of numerical simulations of airflow over real fragments with different mass from projectile 130mm M79 was performed.

Simulations were conducted on two-dimensional fragment models with different angles of attack to simulate fragment rotation.

Research confirmed that fragment slenderness λ (ratio of fragment dimension parallel to velocity vector and fragment dimension perpendicular to velocity vector) is dominant factor influencing drag coefficient C_d value.

This suggests that after the fragmentation of projectile body, fragment with different slenderness are made and during their motion through the air they can have different values of C_d for the same velocity (Ma number).

It means that fragments with identical mass and velocity, but different slenderness, could have different lethality radius.

Comparation of numerical results with available experimental data shows best agreement for supersonic flow regimes and somewhat lower agreement for transonic and subsonic flows.

It is important to remark that velocity of fragments in the lethal zone is always supersonic.

Curve C_d vs Ma, obtained from numerical simulation data, has its peak around 1 Ma, while for other available test data this peak was observed from 1,1 Ma to 1,5 Ma. This difference should be investigated in following research.

Following step in analysis of pressure fields around moving fragments, for different angles of atack, will be defining the difference between center of pressure and center of mass in order to predict fragment overturning moment.

Also, three-dimensional unsteady analysis should be pursued, but these activities require more time and resources.

Because of the complexity of mechanisms involved, further research is needed.

References

[1] ANSYS SYSTEM, Ansys training manuals, www.ansys.com.
[2] Zecevic B., Terzic J., Catovic A.: Analysis of conditions regarding massacre of civilians in square „Kapija“ (Tuzla) on day 25.05.1995, Prossecutors of BiH, december 2007.
[3] Cornell University Fluent Tutorials https://confluence.cornell.edu/display/SIMULATION/FLUENT+Learning+Modules
[4] Ansys Fluent Theory Guide, Ansys System, april 2009.
[5] F. White: Fluid Mechanics, Fourth Edition, McGraw Hill.
[6] B. Zecevic, J. Terzic, A. Catovic, S. Serdarevic-Kadic: Characterization of distribution parameters of fragment mass and number for conventional projectiles, 14th Seminar “New Trends in Research of Energetic Materials”, University of Pardubice, April 13–15, 2011.
[7] A. Ćatović: Assessment of lethal zones for HE warheads with natural fragmentation, Master thesis, July 2007. Sarajevo.
[8] S. B. Pope: Turbulent Flows, Cornell University, Cambridge University Press, 2000.
[9] J. Tu, G. Yeah, C. Liu: Computational Fluid Dynamics, A Practical Aproach, Elsevier, 2008.
[10] F. McCleskey: Drag coefficients for irregular fragments, Naval Surafce Warfare Center, Research and Technology Department and department of Defense, Explosive Safety Board, Dahlgren, Virginia, February, 1988.
[11] N. J. Moga and K. M. Kisielewski: Vertical wind tunnel tests to determine subsonic drag characteristics of unscored warhead fragments, NSWC TR 79-112, Dahlgren, Virginia, May 1979.
[12] J. W. McDonald: Bomb fragments, Eglin Air Force Base, 23 September 1980.
[13] Manual of NATO Safety Principles for the Storage of Military Ammunition and Explosives, NATO/PFP UNCLASSIFIED, AASTP-1 (Edition 1), PART II, May 2006.
[14] TNO Report: General description of the Missile Systems Damage Assessment Code (MISDAC©), Prins Maurits Laboratorium TNO, september 1994.
[15] M. Miller: Drag Coefficient Measurements for Typical Bomb and Projectile Fragments, U. S. Army Research, Development and Engineering Center,Aberdeen Proving Ground, MD, , August 1990.
[16] J. Powell, W. Smith, F. McCleskey: Fragment Hazard Investigation program: Natural Communication detonation of 155mm projectiles, Naval Surface Weapons center, july 1981.
[17] D. Dunn, W. Porter: Air Drag Measurements of Fragments, BRL APG, MD, August, 1955.
[18] R. Ramsey, J. Powell, W. Smith: Fragment Hazard Investigation Program, NSWC TR-3664, Dahlgren, Va, Oct. 1978.
[19] J. D. Anderson, Fundamentals of Aerodynamics, McGraw-Hill Editions, 1991.
[20] A. B. Bailey, J. Hiatt, Free-Flight Measurements of Sphere Drag at Subsonic, Transonic, Supersonic , and Hypersonic Speeds for Continuum, Transition. And Near-Free-Molecular Flow Conditions, Von Karman Gas Dynamics Facility, March 1971.
[21] S. F. Hoerner, Fluid Dynamic Drag, Theoretical, Experimental and Statistical Information, 1965.